TOWARDS QUANTIFICATION OF KIDNEY STONES USING X-RAY DARK-FIELD TOMOGRAPHY

S. Hu⋆†   *F. Yang*‡∗   *M. Griffa*‡   *R. Kaufmann*‡   *G. Anton*§   *A. Maier*⋆†   *C. Riess*⋆

⋆ Pattern Recognition Lab, University of Erlangen-Nuremberg
† Erlangen Graduate School in Advanced Optical Technologies (SAOT), Univ. of Erlangen-Nuremberg
‡ Center for X-ray Analytics and Concrete/Construction Chemistry Laboratory, EMPA
§ Erlangen Centre for Astroparticle Physics (ECAP), University of Erlangen-Nuremberg
∗ Swiss Federal Institute of Technology in Zurich (ETH Zurich), Switzerland

ABSTRACT

Kidney stones is a renal disease with high prevalence and one of the major reasons for emergency room visits. The prevalence of kidney stones is increasing, and the lifetime recurrence rate is estimated as almost 50%. Thus, treatment of kidney stones becomes an increasingly important topic. However, different types of kidney stones require specific treatments, which creates the need for accurate diagnosis of the stone type prior to the intervention. Imaging techniques that are commonly used for the detection of kidney stones, such as X-ray CT and ultrasound, are insufficient to differentiate the types of kidney stones.

In this paper, we present a proof-of-concept study for differentiating kidney stones using X-ray dark-field tomography. The most important advantage of this method is its ability to image non-homogeneous kidney stones, i.e., to localize and identify the individual components of mixed-material kidney stones. We use a weighted total-variation regularized reconstruction method to compute the ratio of dark-field over absorption signal (DA Ratio) from noisy projections. We evaluate the performance of the proposed approach on two kidney stones of homogeneous composition, and one well-defined numerical phantom with known ground truth for mixed types of stones. We illustrate that the DA Ratio is significantly distinguished for different materials from the experiments. Reconstruction of phantom data recovers voxel-wise material information with high accuracy. We show that X-ray dark-field tomography has a significant potential in selective characterization of kidney stones.

Index Terms— X-ray imaging, kidney, Image reconstruction - analytical & iterative methods

1. INTRODUCTION

The kidney stone disease has an estimated prevalence of 13% for men and 7% for women [1] and often leads to emergency department (ED) visits. In U.S., about 1.3 million kidney stone-related ED visits are recorded in 2009 [2]. Both the prevalence and ED visits are increasing [1, 3]. Moreover, current estimates state that nearly half of the patients will have kidney stones again in their lifetime [1]. For a safe and efficient treatment of kidney stones, it is critically important to know the actual type of the stone: for example, non-surgical treatment like lithotripsy and alkalinization can be applied to uric acid stones. Removal of struvite stones oftentimes requires treatment with antibiotics prior to intervention [4, 5].

Various medical imaging techniques have been investigated to classify the types of kidney stones. Conventional CT and sonog-raphy are currently widely used for diagnosing kidney stones, but neither of these two modalities provides good discrimination of the stone type. Dual-energy CT is shown to be a better choice for distinguishing stone types [6, 7, 8]. Recently, researchers explored X-ray dark-field radiography as a new way of imaging and differentiating kidney stones [9]. X-ray dark-field imaging visualizes ultra-small angle scattering of a sample. As such, this imaging technique is sensitive to micro-structural variations at a length scale below the spatial resolution of the images, which enables various new imaging tasks [10, 11]. Technically, such a system can be implemented with a X-ray Talbot-Lau interferometer (TLI). Per pixel, TLI provides the absorption intensity, the first derivative of the phase shift, and a quantity dependent on the ultra-small-angle scattering (the so-called dark-field signal). It has been shown that the ratio of the dark-field signal over absorption (called DA Ratio) is particularly useful to distinguish kidney stones in radiography on the specific examples of uric acid, calcium oxalate, and mixtures thereof [9].

While these first results are promising, radiography suffers from the limitation that it can only measure average signal intensities along the X-ray projection direction. Since most uric stones consist of multiple materials [12, 13], such averages are oftentimes insufficient to classify kidney stones. In this work, we propose X-ray dark-field tomography to localize and quantify mixture materials. We reconstruct absorption and dark-field to compute the DA Ratio per voxel. A statistical analysis shows that the proposed approach effectively distinguishes between different types of stones.

One major challenge for this approach lies in the fact that dark-field projections typically contain high levels of noise. In a TLI setup, for each projection phase stepping is applied to acquire fringe curves from which attenuation, phase shift and dark-field are derived. Any noise in the raw data is typically amplified in the computed dark-field signal [14, 15]. This may lead to inaccurate results for the DA Ratio, which is essential for differentiating mixture components. As a consequence, it is important that the tomographic reconstruction algorithm reduces the noise in the reconstruction and provides a relatively stable result for the DA Ratio computation. To achieve this, we choose an iterative reconstruction approach. Its ability to incorporate prior knowledge is expected to effectively recover information from noisy data [16]. A popular prior is the assumption that the gradient of a natural image are sparse [17]. We apply a weighted total-variation-regularized (wTV) reconstruction algorithm [18, 19] to enhance the sparsity of the data and thus to achieve good performance at high noise levels. Proof-of-concept experiments on two kidney stones of different types and a numerical phantom show the feasibility of the proposed technique.

Fig. 1: Sinogram of the phantom.

Fig. 2: 3-D volume rendering of the mixed stone phantom.

2. RECONSTRUCTION METHODS

The voxel-wise DA Ratio is defined as

$$(\mathbf{r})_{x,y,z} = \frac{(\mathbf{u}^{\mathrm{df}})_{x,y,z}}{(\mathbf{u}^{\mathrm{abs}})_{x,y,z}} \ , \tag{1}$$

where $(\mathbf{u}^{\mathrm{df}})_{x,y,z}$ is the reconstructed dark-field signal and $(\mathbf{u}^{\mathrm{abs}})_{x,y,z}$ is the absorption signal at voxel (x, y, z). Reconstruction of absorption and dark-field signals can be written as the weighted total variation-regularized optimization problem

$$\underset{\mathbf{u}^{\cdot} \in R^n}{\mathrm{argmin}} \|\mathbf{u}^{\cdot}\|_{\mathrm{wTV}} \quad \mathrm{s.t.} \quad \mathbf{A}\mathbf{u}^{\cdot} = \mathbf{p}^{\cdot} \ . \tag{2}$$

Here, $\mathbf{A}$ is the imaging system matrix, $\mathbf{u}^{\cdot}$ denotes the unknown vector collecting absorption or dark-field signals over the whole image, and $\mathbf{p}^{\cdot}$ denotes the observed absorption or dark-field projection signals. For X-ray tomographic reconstruction, $\mathbf{p}^{\cdot}$ acts as a placeholder for either the dark-field $\mathbf{p}^{\mathrm{df}}$ or the absorption $\mathbf{p}^{\mathrm{abs}}$. Both measurements are available at every detector pixel in a Talbot-Lau interferometer. Analogously, the estimated signal is denoted as $\mathbf{u}^{\mathrm{df}}$ or $\mathbf{u}^{\mathrm{abs}}$ respectively, depending on whether they are computed from $\mathbf{p}^{\mathrm{df}}$ or $\mathbf{p}^{\mathrm{abs}}$. The weighted TV norm is defined as

$$\|\mathbf{u}^{\cdot}\|_{\mathrm{wTV}} = \sum_{x,y,z} (\mathbf{W})_{x,y,z} \|(\mathbf{D}\mathbf{u}^{\cdot})_{x,y,z}\|_{2,1} \ . \tag{3}$$

Here, $\mathbf{W}$ is the weight matrix and $\mathbf{D}$ denotes the spatial forward difference operator defined as

$$\mathbf{D} : (\mathbf{u}^{\cdot})_{x,y,z} \mapsto \begin{bmatrix} D_x \\ D_y \\ D_z \end{bmatrix} = \begin{bmatrix} (\mathbf{u}^{\cdot})_{x+1,y,z} - (\mathbf{u}^{\cdot})_{x,y,z} \\ (\mathbf{u}^{\cdot})_{x,y+1,z} - (\mathbf{u}^{\cdot})_{x,y,z} \\ (\mathbf{u}^{\cdot})_{x,y,z+1} - (\mathbf{u}^{\cdot})_{x,y,z} \end{bmatrix},$$

and $\| \cdot \|_{2,1}$ is the isotropic norm

$$\|(\mathbf{D}\mathbf{u}^{\cdot})_{x,y,z}\|_{2,1} = \sqrt{(D_x)^2 + (D_y)^2 + (D_z)^2} \ .$$

The reconstruction problem can be written as

$$\underset{\mathbf{u}^{\cdot} \in R^n}{\mathrm{argmin}} \frac{1}{2}\|\mathbf{A}\mathbf{u}^{\cdot} - \mathbf{p}^{\cdot}\|_2^2 + \lambda\|\mathbf{u}^{\cdot}\|_{\mathrm{wTV}} + l_{\mathcal{R}+}(\mathbf{u}^{\cdot}) \ , \tag{4}$$

where λ is the regularization weight, and $l_{\mathcal{R}+}(\mathbf{u}^{\cdot})$ is the characteristic function of $\mathcal{R}^+$ that constrains the solution to non-negative space [20]. This optimization problem can be solved by primal-dual based iterative algorithms. In our implementation, we use the split-Bregman method by Goldstein *et al.* [21]. Within each iteration, $(\mathbf{W})_{x,y,z}$ is updated by using value of $\mathbf{u}^{\cdot}_{\mathrm{pre}}$ from the previous iteration, i.e.,

$$(\mathbf{W})_{x,y,z} = \frac{1}{\|(\mathbf{D}\mathbf{u}^{\cdot}_{\mathrm{pre}})_{x,y,z}\|_{2,1} + \epsilon} \ , \tag{5}$$

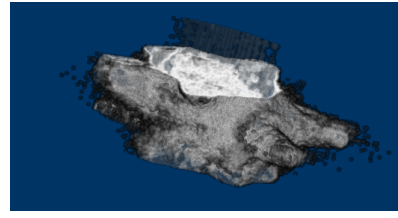and $l_{\mathcal{R}+}(\mathbf{u}^{\cdot})$ is enforced by setting all negative values to zero.

3. EXPERIMENTS

Evaluation is performed on real stones and a numerical phantom. The purpose of the experiments is to show that the DA Ratio allows to distinguish different type of stones. The phantom demonstrates the ability to detect voxel-wise material phases of a mixed stone.

3.1. Pure materials kidney stones

Measurements were performed using one calcium oxalate stone and one struvite stone at the Center for X-ray Analytics, Empa, Switzerland[1]. The imaging setup consists of a X-ray Talbot-Lau interferometer within a micro-focus CT setup. The design energy of the interferometer is $45\,\mathrm{keV}$ at a tube voltage of $80\,\mathrm{keV}$, filtered with $0.5\,\mathrm{mm}$ Al. The detector pixels have a size of $0.2\,\mathrm{mm}$. Two frames are averaged to obtain one image, and a total of seven phase steps are acquired per projection. For tomography, we collect 400 projections on a half circle (π radians).

All stones have diameters between $3\,\mathrm{mm}$ to $5\,\mathrm{mm}$. The reconstruction algorithm is implemented in the CONRAD framework [22]. The value ϵ in Eq. 5 is empirically set to 0.0001. Each data set was reconstructed using 30 iterations. Thresholding was applied to segment the stones from the background.

3.2. Numerical phantom of a mixture of kidney stones

We evaluate the method's ability to localize and quantify the constituents of mixed-type kidney stones on a phantom. The measured stone is used as phantom template, with a volume size of 256^3 voxels. Voxels are in equal parts randomly labeled as calcium oxalate and struvite. The averaged dark-field and absorption signals from the real stones are used as voxel coefficients of the phantom. Forward projection is simulated by linearly accumulating these coefficients along the ray path. A sinogram is generated from 400 projections over a half circle, and Gaussian noise is added with a standard derivation of 0.5. An example sinogram of one slice is shown in Fig. 1. Figure 2 shows a 3-D volume rendering of the full phantom of the ground truth. For reconstruction, we used the same parameters as in the previous experiments.

4. RESULTS AND DISCUSSION

Reconstruction results of the scanned stones are shown in Fig 3. The left column shows absorption images of a representative slice from each stone. The right column shows the respective dark-field images from the same slices. It has been shown via micro-CT scans that less heterogeneity and density variation generate weaker dark-field signals [9]. This observation is confirmed in the reconstruction results:

---

[1]www.empa.ch/x-ray
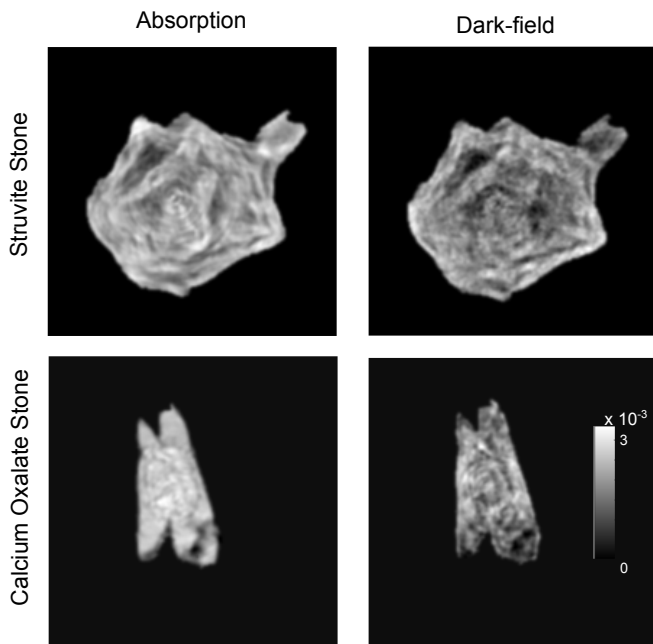
Fig. 3: Top: reconstruction of absorption image (left) and dark-field image (right) of the struvite stone. Bottom: reconstruction of absorption image (left) and dark-field image (right) of the calcium oxalate stone.

Fig. 4: Scatter plot of dark-field versus absorption of one representative slice from the struvite stone (red circle) and the calcium oxalate stone (blue cross).

Fig. 5: Box-whisker diagram of DA Ratio of the whole volume from both stones.

the struvite stone shows a higher mean absorption and lower mean dark-field compared to the calcium oxalate stone.
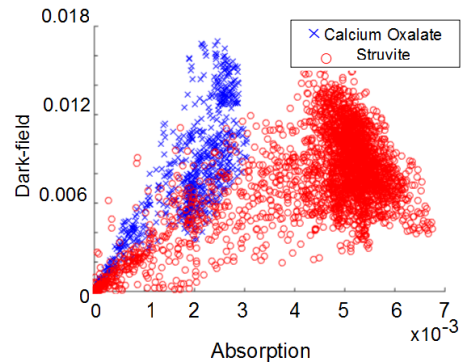
Figure 4 shows a scatterplot of dark-field versus absorption to illustrate the data distribution. Each data point represents one voxel in a representative slice from the reconstruction. Struvite is plotted in red circles, calcium oxalate in blue crosses. Although some points in this plot overlap, the two groups are overall well separated. Most points that are very close to the origin can be explained by remaining noise in the data and ring artifacts in the reconstruction. Struvite signals close to zero exhibit a stronger linear dependency than calcium oxalate. Overall, the slope trends of both sets of data points are clearly distinguishable.

Figure 5 shows a box-whisker diagram of DA Ratio of the whole volume reconstruction of both stones. Around the mean and standard deviations, both groups of data points are cleanly separable. Overall, calcium oxalate results in more outliers (red points).
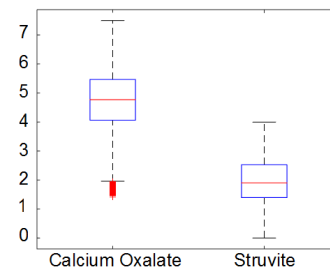
Ground truth and the reconstruction of the representative layer of the phantom is demonstrated in Fig 6. The reconstruction exhibits smoother images compared to the ground truth. One reason for this observation is the noise that has been added to the phantom sinogram. To quantitatively evaluate our result on the phantom data, we calculate the relative root mean square error (rRMSE) as

$$e = \frac{1}{N} \sum_{x,y,z} \sqrt{\frac{((\mathbf{r}^{\mathrm{re}})_{x,y,z} - (\mathbf{r}^{\mathrm{gr}})_{x,y,z})^2}{(\mathbf{r}^{\mathrm{gr}})^2_{x,y,z}}} \ , \qquad (6)$$

where $\mathbf{r}^{\mathrm{re}}$ is the DA Ratio of the reconstructed phantom and $\mathbf{r}^{\mathrm{gr}}$ is that of the ground truth, and N is numbers of voxels of the stone. The resulting RMSE is 1.7%, which is sufficient for differentiating the material phases of the stones.

5. CONCLUSIONS

In this paper, we explore quantification of mixed-type kidney stones using X-ray dark-field tomography. A weighted total variation-regularized optimization algorithm is applied to recover information from noisy input. Experiments show that this approach can distinguish between a struvite and a calcium oxalate stone. We also use a well-defined phantom to study mixed-type kidney stones. Phantom results indicate that the proposed method is able to differentiate different material phases and micro-structures within a mixed-type stone. We conclude that x-ray dark-field tomography is a very interesting potential tool for characterization of kidney stones. However, in the current work, isolated kidney stones have been investigated. In future work, it is necessary to investigate the effectiveness of the proposed approach for kidney stones embedded in surrounding tissue.

6. REFERENCES

[1] M. S. Pearle, E. A. Calhoun, G. C. Curhan, and Urologic Diseases of America Project, "Urologic diseases in America project: urolithiasis," *The Journal of Urology*, vol. 173, no. 3, pp. 848–857, 2005.

[2] G. Foster, C. Stocks, and M. S. Borofsky, *Emergency department visits and hospital admissions for kidney stone disease 2009*, Agency for Health Care Policy and Research (US), 2012.

Absorption   Dark-field

Ground truth
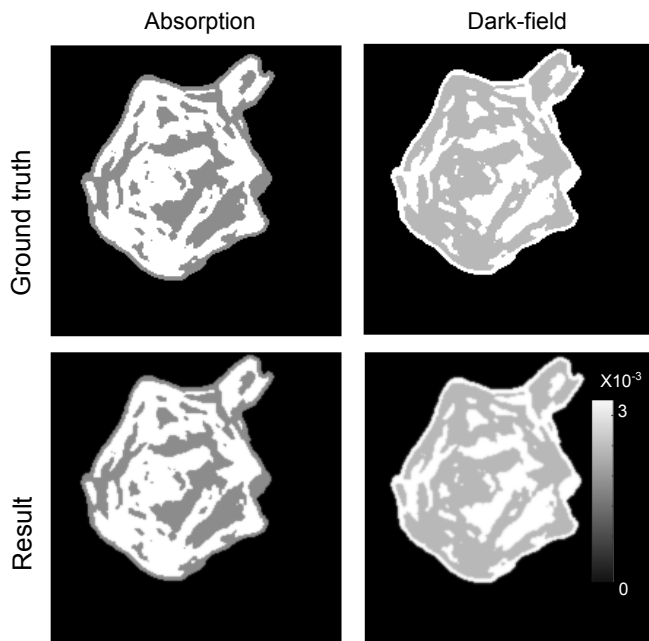
Result

Fig. 6: Top: Bottom: example slice from the ground truth of the mixed stone phantom. Left: absorption, right: dark-field.Reconstruction results of the example slice. Left: absorption signal, right: dark-field signal.

[3] V. Romero, H. Akpinar, and D. G. Assimos, "Kidney Stones: a Global Picture of Prevalence, Incidence, and Associated Risk Factors," *Reviews in Urology*, vol. 12, no. 2-3, pp. e86–e96, 2010.

[4] J. Brown, "Diagnostic and Treatment Patterns for Renal Colic in US Emergency Departments," *International Urology and Nephrology*, vol. 38, no. 1, pp. 87–92, 2006.

[5] N. M. Kulkarni, B. H. Eisner, D. F. Pinho, M. C. Joshi, A. R. Kambadakone, and D. V. Sahani, "Determination of Renal Stone Composition in Phantom and Patients Using Single-Source Dual-Energy Computed Tomography," *Journal of Computer Assisted Tomography*, vol. 37, no. 1, pp. 37–45, 2013.

[6] M.-F. Bellin, R. Renard-Penna, P. Conort, A. Bissery, J.-B. Meric, M. Daudon, A. Mallet, F. Richard, and P. Grenier, "Helical ct evaluation of the chemical composition of urinary tract calculi with a discriminant analysis of ct-attenuation values and density," *European Radiology*, vol. 14, no. 11, pp. 2134–2140, 2004.

[7] P. Stolzmann, M. Kozomara, N. Chuck, M. Müntener, S. Leschka, H. Scheffel, and H. Alkadhi, "In vivo identification of uric acid stones with dual-energy CT: diagnostic performance evaluation in patients," *Abdominal Imaging*, vol. 35, no. 5, pp. 629–635, 2010.

[8] S. Leng, A. Huang, J. M. Cardona, X. Duan, J. C. Williams, and C. H. McCollough, "Dual-Energy CT for Quantification of Urinary Stone Composition in Mixed Stones: A Phantom Study," *American Journal of Roentgenology*, vol. 209, no. 2, pp. 1–9, 2016.

[9] K. Scherer, E. Braig, K. Willer, M. Willner, A. A. Fingerle, M. Chabior, J. Herzen, M. Eiber, B. Haller, M. Straub, H. Schneider, E. J. Rummeny, P. B. Noël, and F. Pfeiffer, "Noninvasive Differentiation of Kidney Stone Types using X-ray

Dark-Field Radiography," *Scientific reports*, vol. 5, pp. 9527, 2015.

[10] F. L. Bayer, S. Hu, A. Maier, T. Weber, G. Anton, T. Michel, and C. P. Riess, "Reconstruction of scalar and vectorial components in X-ray dark-field tomography," *Proceedings of the National Academy of Sciences of the United States of America*, vol. 111, no. 35, pp. 12699–12704, Sept. 2014.

[11] F. Yang, F. Prade, M. Griffa, I. Jerjen, C. Di Bella, J. Herzen, A. Sarapata, F. Pfeiffer, and P. Lura, "Dark-field x-ray imaging of unsaturated water transport in porous materials," *Applied Physics Letters*, vol. 105, no. 15, pp. 154105, 2014.

[12] M. Daudon, C. Hennequin, B. Lacour, G. Le Moel, R. Donsimoni, S. Fellahi, M. Paris, and S. Troupel, "Sex-and age-related composition of 10617 calculi analyzed by infrared spectroscopy," *Urological Research*, vol. 23, no. 5, pp. 319–326, 1995.

[13] M. S. Ansari, N. P. Gupta, A. K. Hemal, P. N. Dogra, A. Seth, M. Aron, and T. P. Singh, "Spectrum of stone composition: structural analysis of 1050 upper urinary tract calculi from northern india," *International Journal of Urology*, vol. 12, no. 1, pp. 12–16, 2005.

[14] M. Chabior, T. Donath, C. David, M. Schuster, C. Schroer, and F. Pfeiffer, "Signal-to-noise ratio in x ray dark-field imaging using a grating interferometer," *Journal of Applied Physics*, vol. 110, no. 5, pp. 053105, 2011.

[15] T. Weber, P. Bartl, F. Bayer, J. Durst, W. Haas, T. Michel, A. Ritter, and G. Anton, "Noise in x-ray grating-based phase-contrast imaging," *Medical physics*, vol. 38, no. 7, pp. 4133–4140, 2011.

[16] H. M. Shieh, C. L. Byrne, M. E. Testorf, and M. A. Fiddy, "Iterative image reconstruction using prior knowledge," *Journal of the Optical Society of America A*, vol. 23, no. 6, pp. 1292–1300, 2006.

[17] M. A. Anastasio E. Y. Sidky and X. Pan, "Image reconstruction exploiting object sparsity in boundary-enhanced x-ray phase-contrast tomographys," *Optics Express*, vol. 18, no. 10, pp. 10404–10422, 2010.

[18] E. J. Candes, M. B. Wakin, and S. P. Boyd, "Enhancing Sparsity by Reweighted L1 Minimization," *Journal of Fourier Analysis and Applications*, vol. 14, no. 5-6, pp. 877–905, 2008.

[19] Y. Huang, O. Taubmann, X. Huang, V. Haase, G. Lauritsch, and A. Maier, "A new weighted anisotropic total variation algorithm for limited angle tomography," in *IEEE International Symposium on Biomedical Imaging: From Nano to Macro*, 2016, pp. 585–588.

[20] L. Condat, "A Generic Proximal Algorithm for Convex Optimization — Application to Total Variation Minimization," *IEEE Signal Processing Letters*, vol. 21, no. 8, pp. 985–989, 2014.

[21] T. Goldstein and S. Osher, "The Split Bregman Method for L1-Regularized Problems," *SIAM journal on imaging sciences*, vol. 2, no. 2, pp. 323–343, 2009.

[22] A. Maier, H. G. Hofmann, M. Berger, P. Fischer, C. Schwemmer, H. Wu, K. Müller, J. Hornegger, J.-H. Choi, C. Riess, A. Keil, and R. Fahrig, "CONRAD — A software framework for cone-beam imaging in radiology," *Medical Physics*, vol. 40, no. 11, pp. 111914, 2013.